A&A 669, A4 (2023)
https://doi.org/10.1051/0004-6361/202244479

Astronomy & Astrophysics

Orbital parallax of binary systems compared to *Gaia* DR3 and the parallax zero-point offset at bright magnitudes⋆

M. A. T. Groenewegen

Koninklijke Sterrenwacht van België, Ringlaan 3, 1180 Brussels, Belgium
e-mail: martin.groenewegen@oma.be

Received 12 July 2022 / Accepted 14 October 2022

ABSTRACT

Multiple systems for which the astrometric and spectroscopic orbit are known offer the unique possibility of determining the distance to these systems directly without any assumptions. They are therefore ideal objects for a comparison of *Gaia* data release 3 (GDR3) parallax data, especially since GDR3 presents the results of the non-single star (NSS) analysis that potentially results in improved parallaxes. This analysis is relevant in studying the parallax zero-point offset (PZPO) that is crucial in improving upon the distance scale. An sample of 192 orbital parallax determinations for 186 systems is compiled from the literature. The stars are also potentially in wide binary systems (WBS). A search was performed and 37 WBS (candidates) were found. Only for 21 objects does the NSS analysis provide information, including 8 from the astrometric binary pipeline, for which the parallaxes do improve significantly compared to those in the main catalogue with significant lower goodness-of-fit (GOF) parameters. It appears that most of the objects in the sample are eliminated in the pre-filtering stage of the NSS analysis. The difference between the orbital parallax and the (best) *Gaia* parallax was finally obtained for 170 objects. A raw comparison is meaningless, however, due to limitations in accuracy both in the orbital and in *Gaia* data. As many systems have been eliminated in the pre-filtering stage of the astrometric NSS pipeline, they remain in GDR3 with values for the GOF parameter in the range from several tens to several hundreds. When objects with large parallax errors or unrealistically large differences between the orbital and *Gaia* parallaxes are eliminated, and objects with a GOF <100 or < 8 are selected (the latter also with $G < 10.5$ mag selected), samples of 68 and 20 stars remain. Parallax differences in magnitude bins and for the sample are presented. Three recipes from the literature that calculate the PZPO are tested. After these corrections are applied the remaining parallax differences are formally consistent with zero within the error bar for all three recipes. In all cases, an uncertainty in these averages of about 10–15 μas remains for these samples due to the small number statistics. The proof of concept of using orbital parallaxes is shown to work, but the full potential is not reached as an improved parallax from the NSS analysis is available for only for eight systems. In the final selection, the orbital parallax of 18 of 20 stars is known to better than 5%, and the parallax determination for 6 stars is better than from *Gaia*. In the full sample, 148 objects reach this precision in orbital parallax and therefore the full potential of using orbital parallaxes may hopefully be reached with GDR4.

Key words. stars: distances – stars: fundamental parameters – parallaxes – binaries: spectroscopic – binaries: visual

1. Introduction

With the second data release (DR; Gaia Collaboration 2018) of the *Gaia* mission (Gaia Collaboration 2016), it was demonstrated that the mean parallax of quasi-stellar objects (QSOs) was not zero, but is slightly negative, −0.029 mas (Lindegren et al. 2018). This was confirmed in the third early DR (GEDR3; Gaia Collaboration 2021), where the average and median parallax zero-point offset (PZPO) of QSOs are −21 and −17 μas, respectively (Lindegren et al. 2021; hereafter L21). L21 presented a Python script to the community that returned the PZPO (without an error bar) as a function of input parameters, namely ecliptic latitude (β), G-band magnitude, the `astrometric_params_solved` parameter, and either the effective wavenumber of the source used in the astrometric solution ($\nu_{\rm eff}$, `nu_eff_used_in_astrometry` for the five-parameter solution `astrometric_params_solved` = 31) or the astrometrically estimated pseudo-colour of the source (`pseudocolour`) for the six-parameter solution (`astrometric_params_solved` = 95). The module is defined in the range $6 < G < 21$ mag, $1.72 > \nu_{\rm eff} > 1.24$ μm^{-1}, corresponding to about $0.15 < (G_{\rm BP} - G_{\rm RP}) < 3.0$ mag where $G, G_{\rm BP}$, and $G_{\rm RP}$ are the magnitudes in the *Gaia* G, Bp, and Rp band, respectively. The script is based on the parallax values of QSOs and wide-binary systems (WBS; see L21 for all details).

In parallel, after the publication of GDR2 numerous studies appeared that studied the PZPO offset using other classes of stars, typically at brighter magnitudes than the QSOs. Examples using GDR2 data are studies of classical cepheids (CCs; Riess et al. 2018; Groenewegen 2018) that found a more negative value (-0.046 ± 0.013 and -0.049 ± 0.018 mas, respectively), RR Lyrae (∼−0.056 mas, Muraveva et al. 2018, -0.042 ± 0.013 mas, Layden et al. 2019), red clump stars (Chan & Bovy 2020), (detached) eclipsing binaries (Stassun & Torres 2018; Graczyk et al. 2019), red giant asteroseismic parallaxes (Zinn et al. 2019; Khan et al. 2019), and stars with parallaxes from very long baseline interferometry (Xu et al. 2019), amongst others. With the advent of GEDR3 this line of research has continued (Huang et al. 2021; Stassun & Torres 2021; Ren et al. 2021; Zinn 2021; Riess et al. 2021; Maíz Apellániz 2022, hereafter MA22), including claims that the L21 procedure overcorrects the PZPO (Riess et al. 2021; Zinn 2021), at least for brighter objects. Alternative procedures for the L21 correction have been proposed by

⋆ Full Tables 1 and 2 are available at the CDS via anonymous ftp to cdsarc.cds.unistra.fr (130.79.128.5) or via https://cdsarc.cds.unistra.fr/viz-bin/cat/J/A+A/669/A4

Groenewegen (2021, hereafter G21) and MA22. Clearly, the spatial, magnitude, and colour dependence of the PZPO remains of great interest.

One disadvantage of using alternative classes of objects is the intrinsic assumption is that the distances to those objects are known exactly, and with an accuracy comparable to that of *Gaia*. However, with the exception of the QSOs that truly have a parallax of zero for all practical purposes, this is based on direct or indirect assumptions or model dependences, such as reddening, a (linear) period-luminosity relation, an absolute magnitude, or a surface-brightness colour relation.

Binaries for which the astrometric and spectroscopic orbits are known offer the possibility of deriving the orbital parallax free from any assumption, based on Kepler laws. The only limitation in the accuracy of the distance is ultimately the quality of the data. GDR3 (Gaia Collaboration 2023b) offers the possibility of comparing *Gaia* trigonometric parallaxes to orbital parallaxes. In previous releases, the *Gaia* astrometric solution assumed single stars. Therefore, the quality parameters of the astrometric solution, such as the goodness of fit (GOF, `astrometric_gof_al`) or the renormalised unit weight error (`RUWE`), were (very) poor for (close) binary systems. In GDR3, non-single star (NSS) solutions are considered (Halbwachs et al. 2023; Gaia Collaboration 2023a), which means that for a subset of stars, (improved) parallaxes are determined that binary motion into account. Individual studies of astrometric and spectroscopic binary orbits also often derived the orbital parallax and compared it to HIPPARCOS or *Gaia* data, but no real systematic differences can be identified as the PZPO is a small quantity using mostly single objects (Gallenne et al. 2019 used four objects in the comparison of the orbital parallax and GDR2 data).

The paper is structured as follows. In Sect. 2, the sample of binaries is introduced and confronted with G(E)DR3 data. The impact and limitations of the DR3 NSS analysis are discussed in Sects. 3.1 and 3.2, and the PZPO is discussed in Sect. 3.3. A brief discussion and summary conclude the paper.

2. Sample

Recently, Piccotti et al. (2020) compiled a list of 69 SB2s with both visual and spectroscopic orbits, but the emphasis of that paper was on the masses and ages of the systems. The sample selection followed that of Piccotti et al. (2020) and was based on an extensive literature search using the Sixth Catalogue of Orbits of Visual Binary Stars (ORB6; Hartkopf et al. 2001, starting from orbits with grades 1, 2, and 3)[1] and the Ninth Catalogue of Spectroscopic Binary orbits (SB9; Pourbaix et al. 2004)[2]. This initial correlation pointed to other literature that was then searched. Articles by specific authors were searched through the ADS, and the arXiv was monitored for relevant papers. The literature search ended May 10, 2022. Table 1 lists the adopted orbital elements and velocity amplitudes with references for a total of 186 systems. For six binaries, several components have been resolved (WDS 03272+0944, 06024+0939, 06290+2013, 17247+3802, 20396+0458, and 22388+4419), and therefore the table has 192 entries. This almost triples the number of systems compared to Piccotti et al. (2020). Although it was attempted to make this list complete, this cannot be guaranteed. Obviously, GDR3 provides orbital elements and velocity amplitudes for selected systems, and the impact of this is discussed in Sect. 3.2.

[1] `http://www.astro.gsu.edu/wds/orb6/orb6frames.html`
[2] `https://sb9.astro.ulb.ac.be`

The orbital parallax follows from the orbital elements as

$$\pi_{\rm o} = a/\left((K_1 + K_2) \cdot P/29.7847 \cdot \sqrt{1-e^2}/\sin i\right) \quad (1)$$

where a is the semi-major axis in mas, K_1 and K_2 are the velocity semi-amplitudes of the two components (in km s^{-1}), P is the orbital period in years, e is the eccentricity of the orbit, i is the inclination in degrees, and $\pi_{\rm o}$ is the orbital parallax in mas. The error in $\pi_{\rm o}$ is calculated through standard error propagation assuming all errors are independent. The orbital parallaxes and errors are listed in Table 2.

No selection on the accuracy of period, major axis, inclination, or velocity amplitude is made to be included in the sample, even if a large error implies a large error on the orbital parallax and likely a value that is not competitive in accuracy with the *Gaia* value. For objects for which no error bars on the orbital elements was published, an error of 1.3, 6, and 40% on period, 2.5, 15, and 40% on a, 5, 12, and 27° on i, and 0.01, 0.02, and 0.10 on e was adopted for orbits of grade 1, 2, and 3 in ORB6, respectively. If no error on the velocity amplitude was reported, an error of 5% was adopted. These cases are marked in Table 1 and are good targets for further observations to improve on the orbital parameters.

As a first step and as preparation for the DR3 release, the objects were identified in GEDR3 and also in the HIPPARCOS catalogue (the new reduction version by van Leeuwen 2008). The later proved essential in many cases as the epoch 1991.25 HIPPARCOS coordinates could be transformed to the epoch 2016.0 of GEDR3/GDR3 to properly identify the correct object that was achieved by comparing coordinates, parallax, and magnitude. It was then trivial to identify the correct object with the release of DR3, and Table 2 gives the orbital parallax (based on the data in Table 1 and Eq. (1)), and some information from HIPPARCOS and DR3 for the 192 objects. DR3 includes some parameters that were used in the pre-filtering stage of the astrometric binary pipeline (Halbwachs et al. 2023); they are discussed in detail below.

Inspection of Table 1 reveals that quite a number of objects (59, or about 30%) are not listed in GDR3, or are listed without parallax. The former are six of the very brightest objects (all have $V \lesssim 2.7$ mag). The others only have two-parameter solutions (`astrometric_params_solved = 3`). However, these objects may potentially be in WBS. To investigate this further, the objects were correlated with the catalogue of El-Badry et al. (2021, based on GEDR3 data). Fourteen matches were found at distances up to 57″. However, objects without a parallax or proper motion in GEDR3 are obviously missing from El-Badry et al. (2021). In a second step, all sources within 1′ were retrieved from GDR3 and a potential list of WBS was compiled based on the orbital parallax and criteria on the parallax difference so that the search would retrieve all 14 matches in El-Badry et al. (2021). In a final step, the GDR3 and HIPPARCOS parallaxes and proper motions were inspected to make a final list of likely WBS, keeping only stars with Bp and Rp photometry. The information of these 37 sources is listed in Table A.1.

3. Results

3.1. Effects of pre-filtering in the NSS processing

Table A.2 shows that only 21 of the 180 (186 unique objects minus 6 stars not in DR3) known binaries have a non-zero NSS flag. In other words, 90% of the known binaries have not been

Table 1. Sample of stars (selected entries).

Name	HD	Period	σ_P	u	a ($''$)	σ_a ($''$)	i ($^\circ$)	σ_i ($^\circ$)	e	σ_e	K_1 (km s^{-1})	σ_{K_1} (km s^{-1})	K_2 (km s^{-1})	σ_{K_2} (km s^{-1})	Reference
00084+2905	358	96.7015	0.0044	d	0.02400	0.00013	105.60	0.23	0.5348	0.0046	27.74	0.55	65.47	0.96	Pourbaix (2000)
00369+3343	3369	143.53	0.06	d	0.006690	0.000050	103.0	0.2	0.5420	0.0060	47.50	0.53	117.4	2.8	Pearce (1936) Hummel et al. (1995)
00373−2446	3443	9165.640	10.592	d	0.6750	0.0169*	78.6	5.0*	0.2352	0.0096	5.13	0.29	6.93	0.22	Pourbaix (2000)
00490+1656	4676	13.82462	0.00002	d	0.006527	0.000061	73.80	0.92	0.2376	0.0012	57.35	0.31	59.95	0.32	Boden et al. (1999)
01028+3148	6118	81.12625	0.00027	d	0.005560	0.000040	143.4	1.3	0.8956	0.0020	53.2	1.9	59.6	1.6	Konacki & Lane (2004)
01096−4616		24.59215	0.00002	d	0.001315	0.000005	91.32	0.39	0.1872	0.0001	51.166	0.008	49.118	0.007	Gallenne et al. (2019)
01108+6747	6840	2722.0	1.0	d	0.08300	0.01245*	52.0	12.0*	0.7442	0.0020	11.18	0.06	12.34	0.12	Griffin (2012b) Docobo et al. (2018b)
01237+3743	8374	35.36836	0.00005	d	0.005050	0.000020	140.64	0.45	0.6476	0.0005	39.27	0.05	40.47	0.05	Lester et al. (2020)
01277+4524	8799	254.9003	0.1960	d	0.0380	0.0010	62.49	2.10	0.142	0.012	17.54	0.30	19.62	0.30	Farrington et al. (2014)
01321+1657	9312	36.51836	0.00068	d	0.0030	0.0012*	65.4	13.3	0.1429	0.0003	34.972	0.006	45.821	0.065	Wang et al. (2015) Kiefer et al. (2018)
01374+2510	9939	25.20896	0.00007	d	0.004944	0.000018	61.56	0.25	0.10166	0.00097	34.952	0.055	44.68	0.24	Boden et al. (2006)
01376−0924	10009	28.83	0.25	y	0.2920	0.0090	97.4	0.2	0.748	0.005	9.16	0.21	11.21	0.32	Tokovinin (1993)
01379−8259	10800	1.74861	0.00047	y	0.07823	0.00047	47.60	0.48	0.1912	0.0018	9.10	0.03	17.91	0.05	Tokovinin (2016b)
01437+5041	10516	126.6982	0.0035	d	0.005890	0.000020	77.6	0.3	0.00000	0.1*	10.2	1.0	81.5	0.7	Mourard et al. (2015)
01546+2049	11636	106.99442	0.00069	d	0.03600	0.00016	47.50	0.54	0.8801	0.0008	37.10	1.86*	66.60	3.33*	Pourbaix (2000) Tokovinin (2016b)
02057−2423	12889	2.582	0.003	y	0.0480	0.0030	75.9	4.0	0.769	0.015	18.52	0.50	19.10	0.50	Tokovinin et al. (2014)
02128−0224	13612	0.25952	0.00001	y	0.01398	0.00075	25.6	7.8	0.6920	0.0027	19.01	0.04	19.74	0.43	Anguita-Aguero et al. (2022)
02171+3413	13974	10.02000	0.00010	d	0.009800	0.000060	167.0	3.0	0.0200	0.0050	10.52	0.17	11.85	0.40	Hummel et al. (1995) Pourbaix (2000)
02211+4246		318.0	17.0	y	0.940	0.022	147.0	2.3	0.8020	0.0072	1.90	0.57	2.92	0.57	Pourbaix (2000)
02262+3428	15013	2533.0	5.0	d	0.0990	0.0149*	49.9	12.0*	0.300	0.005	7.61	0.06	7.86	0.07	Docobo et al. (2018a) Griffin (2018)
02278+0426	15285	9182.4	14.6	d	0.5429	0.0052	73.0	0.7	0.210	0.010	5.60	0.30	6.40	0.30	Agati et al. (2015)
02415−7128	17215	106.3	4.6	y	0.568	0.012	114.7	0.4	0.384	0.020	4.12	0.44	4.69	0.88	Tokovinin (2022)
02422+4012	16739	330.9910	0.0044	d	0.05318	0.00015	128.17	0.14	0.6630	0.0021	20.912	0.089	23.730	0.087	Pourbaix (2000) Bagnuolo et al. (2006)
02442−2530	17134	6.68917	0.00510	y	0.10020	0.00060	42.00	0.72	0.4999	0.0015	7.440	0.041	8.050	0.041	Tokovinin (2016a)
02539−4436	18198	51.46	0.82	y	0.2967	0.0044	49.5	1.9	0.774	0.013	3.98	0.61	9.93	0.70	Tokovinin (2016b)
03025−1516	18955	43.32032	0.00013	d	0.005810	0.000034	92.24	0.18	0.7594	0.0010	54.31	0.29	60.45	0.34	Halbwachs et al. (2016)
03048+5330	18925	14.5930	0.0046	y	0.14390	0.00073	90.60	0.71	0.7860	0.0038	13.67	0.22	18.57	0.31	Pourbaix (1999) Pourbaix (2000)
03082+4057	19356	680.168	0.046	d	0.09343	0.00011	83.66	0.03	0.2270	0.0020	12.00	0.40	31.60	1.20	Hill et al. (1971) Baron et al. (2012)
03147−3533	20301	75.66691	0.00019	d	0.002990	0.000011	85.71	0.04	0.00000	0.00010	38.91	0.01	40.88	0.01	Gallenne et al. (2018)
03272+0944	21364	145.113	0.071	d	0.01593	0.00010	86.67	0.12	0.2101	0.0053	43.160	2.410	38.370	0.190	Nemravová et al. (2016)
03272+0944	21364	7.14664	0.00002	d	0.00189	0.00011	86.85	0.22	0.01	0.10*	87.79	0.25	93.02	0.23	Nemravová et al. (2016)
03396+1823	22694	0.826	0.003	y	0.02250	0.00080	128.31	4.98	0.577	0.004	14.16	1.44	15.39	1.57	Jao et al. (2016)
03400+6352	17126	11.42	0.08	y	0.1460	0.0020	70.0	20.0*	0.475	0.016	7.22	0.14	9.95	0.36	Tokovinin et al. (2019)
03566+5042	24546	30.43885	0.00002	d	0.00699	0.00006	56.76	0.45	0.6421	0.0006	52.24	0.06	53.15	0.06	Lester et al. (2020)
04107−0452	26441	20.6290	0.0077	y	0.16472	0.00066	67.94	0.18	0.8400	0.0014	11.61	0.04	12.41	0.06	Anguita-Aguero et al. (2022)
04142+2813	283447	51.1003	0.0022	d	0.002837	0.000035	63.3	1.1	0.2710	0.0072	35.74	0.66	43.00	1.40	Torres et al. (2012)
04184+2135	27176	11.3642	0.0071	y	0.13537	0.00016	123.88	0.25	0.1540	0.0016	7.50	0.32	8.96	0.11	Anguita-Aguero et al. (2022)
04209+1352	27483	3.05911	0.00001	d	0.00126	0.00005	45.1	1.7	0.0	0.1*	71.55	0.27	72.88	0.38	Konacki & Lane (2004) Griffin (2012a)
04247+0442	27935	156.38052	0.00009	d	0.011338	0.000022	103.133	0.072	0.85128	0.00003	37.335	0.003	50.322	0.040	Halbwachs et al. (2020)
04256+1556	27991	2295.0	4.0	d	0.1000	0.0031	125.0	1.6	0.7155	0.0097	11.24	0.19	13.61	0.15	Pourbaix (2000) Griffin (2012a)
04268+1052	286820	19.77	0.27	y	0.201	0.010	63.0	2.2	0.649	0.040	6.80	0.34*	9.50	0.48*	Tokovinin (2021) Griffin (2012a)

Notes. Column 1: The identifier used in this paper. It follows the WDS convention. Column 2: HD number. Columns 3–5: Pulsation period, error and unit (y = years, d = days, h = hours, m = minutes). An asterisk in Columns 5, 7, 9, 11, 13, or 15 indicates that the error bar was assumed. Columns 6 and 7: Semi-major axis and error in arcsec. Columns 8 and 9: Inclination and error in degrees. Columns 10 and 11: Eccentricity and error. Columns 12–15: Semi-amplitude of the velocity with error, for both components. Column 16: References. In the electronic version the values for the orbital parameters are given at fixed formats which implies that the number of significant digits is sometimes too large.

Table 2. Parallax data (selected entries).

Name	π_o (mas)	HIP	π (mas)	GOF	H_p (mag)	Source ID	π (mas)	GOF	RUWE	G-mag (mag)	NSS	ipdfmp (%)	ipdha	Nv	signiC*
00084+2905	33.019 ± 0.428	677	33.62 ± 0.35	11.77	2.04										
00369+3343	3.565 ± 0.066	2912	5.45 ± 0.31	5.82	4.31	3649362286114675 20	5.656 ± 0.147	0.72	1.02	4.30	0	0	0.03	16	0.052
00373−2446	67.002 ± 2.608	2941	64.93 ± 1.85	28.19	5.71	2347260998051944448		103.56	0.00	5.95	0	99	0.24	3	131.180
00490+1656	43.289 ± 0.437	3810	42.64 ± 0.27	1.30	5.18	2781872793183604096	42.751 ± 0.112	0.21	1.01	4.93	2	0	0.03	14	1.523
01028+3148	8.859 ± 0.203	4889	7.52 ± 0.26	1.51	5.49	3141420555832439 04	8.454 ± 0.096	−1.00	0.94	5.49	0	0	0.02	14	0.580
01096−4616	5.904 ± 0.022	5438	3.50 ± 1.04	–0.45	8.74	4933562966514402176	5.907 ± 0.019	4.86	1.15	8.43	2	0	0.05	26	0.474
01108+6747	16.639 ± 2.626	5531	18.30 ± 0.53	3.75	6.67	5265373967862947 84	16.924 ± 0.156	116.57	8.62	6.42	0	0	0.03	24	2.093
01237+3743	16.213 ± 0.066	6514	15.66 ± 0.30	–0.41	5.67	3231596314792185 60	15.762 ± 0.127	–0.20	0.99	5.54	0	0	0.02	13	0.510
01277+4524	39.106 ± 1.121	6813	34.94 ± 0.31	2.17	4.92	3973723713884554 24	34.733 ± 0.134	5.59	1.33	4.69	0	14	0.03	14	3.179
01321+1657	10.162 ± 4.083	7143	17.32 ± 0.50	0.80	6.94	2592750264855961472	17.730 ± 0.060	39.54	2.66	6.54	0	0	0.04	15	0.072
01374+2510	23.683 ± 0.113	7564	22.55 ± 0.56	1.40	7.15	2920697376125876 48	22.510 ± 0.041	15.55	1.90	6.76	0	0	0.03	13	0.125
01376−0924	22.128 ± 0.818	7580	24.76 ± 0.90	1.96	6.35	2464859126762143616	22.970 ± 0.630	217.16	20.70	6.13	0	6	0.19	16	3.565
01379−8259	37.116 ± 0.237	7601	36.52 ± 0.28	2.45	6.01	4618008180223988352	37.013 ± 0.229	75.55	7.28	5.70	0	0	0.02	18	2.863
01437+5041	5.387 ± 0.078	8068	4.54 ± 0.20	–1.33	3.98	4059875260298512 64	5.405 ± 0.197	13.53	1.80	4.08	0	0	0.08	15	6.557
01546+2049	54.813 ± 1.974	8903	55.60 ± 0.58	28.01	2.70										
02057−2423	22.331 ± 1.457	9774	21.44 ± 1.43	2.07	8.70	5121561656518510080	21.089 ± 0.088	39.98	3.00	8.41	0	72	0.16	17	23.693
02128−0224	24.783 ± 2.616	10305	25.19 ± 1.41	25.87	5.77	2494066897240089728	26.538 ± 0.127	28.82	3.28	5.54	0	0	0.02	11	1.491
02171+3413	107.018 ± 6.048	10644	92.73 ± 0.39	5.00	4.98	3261730449575180 80	91.650 ± 0.427	26.48	3.25	4.67	0	0	0.15	10	2.039
02211+4246	16.655 ± 2.660	10952	17.98 ± 1.38	1.66	8.93	3393842956421982 72	15.417 ± 0.236	35.90	4.20	9.19	0	52	0.10	10	150.764
02262+3428	22.039 ± 3.510	11352	24.31 ± 0.99	1.67	8.15	3269401647743683 84	22.494 ± 0.136	71.40	6.23	7.82	0	0	0.10	15	0.740
02278+0426	52.428 ± 1.879	11452	58.33 ± 1.08	–0.53	8.78	2515752565074318720		1267.22	0.00	8.50	0	84	0.18	10	111.003
02415−7128	17.775 ± 2.001	12548	18.60 ± 0.81	2.52	7.90	4644298430956871040		574.00	0.00	7.63	0	36	0.21	24	6.940
02422+4012	41.119 ± 0.163	12623	41.34 ± 0.43	8.42	5.02	3351448923373263 36	41.796 ± 0.296	20.27	2.75	4.72	0	0	0.17	10	7.530
02442−2530	22.253 ± 0.158	12780	24.20 ± 1.16	8.22	7.09	5076722404106123264	21.676 ± 0.293	190.55	13.87	6.82	0	1	0.01	21	1.372
02539−4436	14.826 ± 0.998	13498	14.09 ± 0.73	1.99	7.84	4755117967402573056	11.965 ± 0.368	227.03	18.02	7.71	0	61	0.14	22	29.454
03025−1516	19.526 ± 0.137	14157	19.78 ± 1.10	0.69	8.59	5154084145316239744	19.446 ± 0.052	14.83	1.86	8.23	0	0	0.01	15	0.106
03048+5330	14.735 ± 0.188	14328	13.41 ± 0.51	20.17	3.06	447071293401293056	14.125 ± 0.768	134.43	10.85	2.65	0	1	0.06	18	47.001
03082+4057	34.978 ± 0.990	14576	36.27 ± 1.40	52.82	2.10										
03147−3533	5.373 ± 0.020	15092	5.75 ± 0.51	2.80	7.02	5047189109469319680	5.471 ± 0.019	9.10	1.31	6.68	2	0	0.01	27	0.738
03272+0944	14.957 ± 0.441	16083	15.60 ± 1.04	31.49	3.71	12730974556132096	16.791 ± 0.694	61.89	7.28	3.70	0	57	0.04	11	1.088
03272+0944	15.889 ± 0.929	16083	15.60 ± 1.04	31.49	3.71	12730974556132096	16.791 ± 0.694	61.89	7.28	3.70	0	57	0.04	11	1.088
03396+1823	26.378 ± 2.052	17076	25.61 ± 1.34	1.84	8.39	5686169480405312 0	27.449 ± 0.027	1.36	1.06	8.03	2	0	0.02	15	0.480
03400+6352	23.682 ± 1.927	17126	24.59 ± 1.05	–0.03	8.43	4880992605516587 52	24.067 ± 0.573	472.07	28.84	8.06	0	4	0.06	22	4.136
03566+5042	25.862 ± 0.223	18453	26.71 ± 0.87	17.82	5.38	2504373139465913 60	26.217 ± 0.082	1.10	1.04	5.17	2	0	0.03	17	1.594
04107−0452	16.912 ± 0.085	19508	16.09 ± 0.65	1.48	7.50	3203497397487659648	17.289 ± 0.538	252.83	24.68	7.23	0	0	0.01	17	2.686
04142+2813	7.119 ± 0.163	19762	10.45 ± 2.68	3.26	10.86	1631843661308099 84	8.326 ± 0.131	119.48	7.53	9.99	0	0	0.01	18	1.568
04184+2135	18.111 ± 0.367	20087	18.50 ± 0.50	6.75	5.71	4951056621894476 8	19.505 ± 0.239	80.83	5.03	5.55	0	0	0.06	14	3.658
04209+1352	21.976 ± 0.882	20284	21.09 ± 0.51	3.45	6.26	3310615565476268032	21.093 ± 0.033	2.22	1.12	6.05	0	0	0.03	12	0.307
04247+0442	16.700 ± 0.033	20601	15.20 ± 1.35	–0.21	9.06	3283823387685219328	17.308 ± 0.119	85.37	6.44	8.73	1	0	0.03	16	0.245
04256+1556	22.366 ± 0.728	20661	21.20 ± 0.92	8.42	6.56	3312783561888068352	21.108 ± 0.496	343.28	23.99	6.34	0	0	0.08	18	2.622
04268+1052	21.758 ± 1.356	20751	24.11 ± 1.59	0.71	9.58	3306007129990778368	21.159 ± 0.395	227.23	22.14	9.10	0	1	0.03	16	1.134

Notes. Column 1: Identifier used in this paper. Column 2: Orbital parallax. Columns 3–6: HIPPARCOS data: HIP number, parallax, GOF, H_p magnitude. Columns 7–16: GDR3 data: Source identifier, parallax, GOF, RUWE, G magnitude, Non-Single-Star (NSS)-flag, ipdfm (`ipd_frac_multi_peak`), idpha (`ipd_gof_harmonic_amplitude`), Nv (`visibility_periods_used`). The last column is the significance of the modified Bp-Rp excess (C*), calculated according to Riello et al. (2021).

flagged as such by the NSS pipeline(s). Although this is the reality of the current release, it might be instructive to investigate how these binaries were overlooked. Halbwachs et al. (2023) described the processing of astrometric binary stars. Stars were selected to be brighter than $G = 19$ mag and have 12 or more visibility periods. The first criteria has no impact, and the second removes 23 objects. There is a selection on keeping sources with RUWE < 1.4, removing 93 objects (of the 130 that have a RUWE listed), on `ipd_frac_multi_peak` ≤ 2, removing 64 objects, on `ipd_gof_harmonic_amplitude` <0.1, removing 57 objects, and on the significance of the modified Bp-Rp excess, $|C^\star|/\sigma_{C^\star} < 1.645$, removing 113 objects.

Only 30 objects meet all pre-selection criteria. Additional objects are likely to have been removed in the processing and the post-processing steps (see details in Halbwachs et al. 2023). Similar criteria must have been adopted in the processing of spectroscopic binaries, but the paper describing this has not been published at the time of submission. As the aim of the paper is to use improved parallaxes from the astrometric binary pipeline, the details of the processing in the spectroscopic binary pipeline are less relevant here.

3.2. Comparing the orbital elements of the NSS processing with the literature

Comparison of the orbital elements in Table A.2 with those in the literature reveals that a number of them (03396+1823, 04179−3348, 12313+5507, 17038−3809, 17422+3804, 18339+5144, 23456+1309, 23485+2539, and 18339+5144) refer to a different component than listed in Table 1, because period, eccentricity or velocity amplitude do not match. In all cases except one, the period in Table A.2 is the shorter one, suggesting that the elements refer to some inner orbit of the multiple system. Consultation of the ORB6 suggests that none of these orbits was known.

In the other cases, the elements found by the NSS analysis are not more precise than known in the literature, which were therefore kept. The median and 1.4826× median absolute deviation (MAD; equivalent to 1σ in a Gaussian distribution) were calculated of $(x_1 - x_2)/\sqrt{\sigma^2_{x_1} + \sigma^2_{x_2}}$, where x represents period, eccentricity, or the velocity amplitudes, from the literature and the NSS analysis, and which are expected to be zero and unity, respectively.

Although the sample is small the errors on the parameters in the SB2 solution appear to be underestimated, as is indeed suggested at the end of Sect. 6 in Babusiaux et al. (2023). When we take the formal errors, the width of the distribution is about $4–9\sigma$. When the errors are Scaled with $\sqrt{\mathrm{GOF}}$, this is reduced to $0.8–1.5\sigma$. For the non-SB2 solutions, the width is $0.6–1.6\sigma$, suggesting that the error estimates are realistic.

3.3. PZPO

The main aim of the paper is to the investigate the PZPO. Figure 1 shows the difference of DR3 parallax minus orbital parallax for the objects plotted against G magnitude. The range in ordinate is ±12 mas to display all points. The *Gaia* parallax is the improved parallax from the NSS analysis (with its associated GOF parameter) for the eight stars in Table A.2 and from Table 1 otherwise. Added are the 37 WBS from Table A.1 for a total of 170 determinations plotted. When two *Gaia* parallaxes were available (from the counterpart of the orbital parallax source and from a WBS), they were not averaged as the PZPO depends on

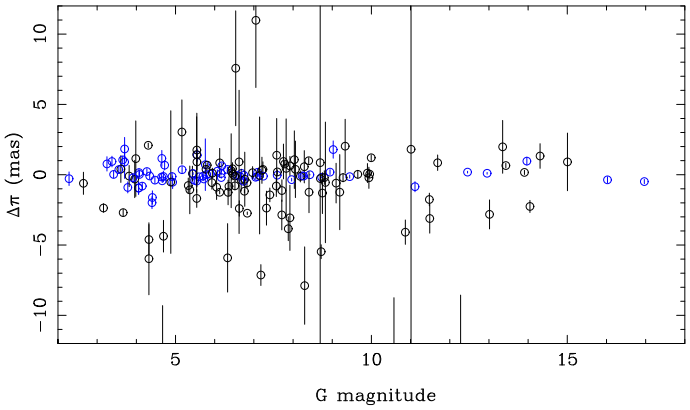

Fig. 1. Parallax difference in the sense DR3 minus orbital parallax for the entire sample. The range in ordinate is ±12 mas. The stars from the SS are plotted in blue (see text).

magnitude and possibly on colour. The figure shows that some of the parallax errors (dominated by the error in orbital parallax) are large and do not constrain any difference with the DR3 parallaxes. Unless specified otherwise, a standard selection (SS) is applied from now on choosing objects where the error in the orbital parallax should be smaller than five times the error in the DR3 parallax, the error in the orbital and DR3 parallaxes should be smaller than 2 mas, the ratio of the absolute difference between orbital and DR3 parallax to the combined error bar should be lower than five, and the GOF (either from the astrometric solution or the NSS solution) should be lower than 100, reducing the number of points to 68. In Fig. 1, these points are plotted in blue, and Fig. 2 shows a zoom with ordinates of ±0.15 mas using this selection. The data were also binned in G mag, using five bins that started at $G = 0$, 5.0, 6.0, 7.4, and 9.2 mag (this last bin includes all fainter objects), where the weighted mean (and error on the mean) was calculated, and plotted at the mean G magnitude of the objects in that bin. The first bin collects all of the brightest objects. Bright limits of 5.0 and 6.0 mag were used in G21 and L21/MA22, respectively, while 7.4 and 9.2 mag are cardinal magnitudes used in MA22. The weighted average over all objects results in an offset of -41.7 ± 10.7 μas (model 1 in Table 3, which also includes the values per magnitude bin).

Several corrections to the G(E)DR3 parallaxes have been proposed, and it is interesting to compare the corrected parallaxes to the orbital ones. To guide the eye, the solid line in Fig. 2 shows the magnitude correction from G21 with a constant spatial offset of −0.013 mas added (the average spatial correction of the sample following G21 at HEALPix level 0). We recall that the HEALPix formalism (Górski et al. 2005) is a convenient way to divide the sky into equal-area pixels. At HEALPix level 0, there are 12 pixels, and this increases by a factor of four for every next higher level. The HEALPix formalism is used by the *Gaia* team and is encoded in the `source_id`[3].

Below, we apply different corrections on a star-by-star basis to the GDR3 parallaxes. If the corrections work the weighted mean difference should be consistent with zero. The first correction is the one by L21 (model 2). The number of sources is reduced to 30 as the correction is only defined for stars fainter than magnitude 6. After correction, the difference with the orbital parallax is -8.7 ± 11.5 μas. Model 3 shows the results

[3] Pixel number = `source_id`/$(2^{35} \cdot 4^{(12-\mathrm{level})})$ for a given HEALPix level.

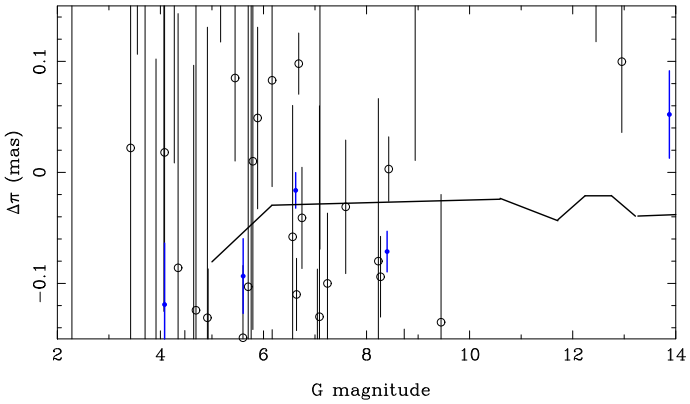

Fig. 2. Zoom of Fig. 1, with the SS applied as described in the text. There are points outside the plot range. The blue points are the weighted averages plotted at the mean magnitude of the objects in the magnitude bins. The solid lines represent the magnitude dependence of the PZPO from G21 with an average spatial correction of −0.013 mas added.

for the MA22 correction, which is an extension of L21. The resulting difference is marginally closer to zero. We note that the errors on the correction are identical to applying no correction. This is related to the fact that the L21 and MA22 provided the offset without error bars. Finally, the G21 formalism was tested. The correction depends on the chosen HEALPix level and consists of a spatial correction defined at $G = 20$ mag (depending on the source coordinates (i.e. a certain pixel) at a chosen HEALPix level) and an additive magnitude correction. Following G21, only pixels with more than 40 QSOs have been considered. Models 4–8 show the results for HEALPix levels 0–4, respectively. As the G21 correction is defined for $G > 5$, there are more objects at the lower HEALPix levels, but then the number decreases with increasing HEALPix level as the number of objects in pixels with insufficient QSOs increases. HEALPix level 2 seems a good compromise between the sampling of the spatial correction and the loss of objects, and the result is comparable to the results for the other correction methods. If the G21 correction is limited to $G > 6$ mag, as it is for the other two methods, the resulting difference is very close to zero (model 6a).

The SS is useful to obtain insight into the overall behaviour of the PZPO but now a stricter final selection (FS) is introduced. As there are few objects fainter than tenth magnitude that nevertheless cover a wide range, and because there are very few extremely bright objects, the sample was restricted in magnitude and two bins from 4–6.162 and 6.162–10.591 mag (two breakpoints in Eq. (7) in G21) were considered. As there is a general offset between orbital and *Gaia* parallaxes, the condition on the difference of the two was modified to $|(\pi_{Gaia} - (-0.04\ \mathrm{mas})) - \pi_{\mathrm{orb}}|/\sigma_c < 5.0$, where σ_c is the combined error of the *Gaia* and the orbital parallax $\sqrt{(k \cdot \sigma_{\pi_{Gaia}})^2 + \sigma^2_{\pi_{\mathrm{orb}}}}$. The factor k is the error inflation factor, which was set to unity in the SS. Several papers have found that the error bars in the astrometric solution are underestimated (Fabricius et al. 2021; Maíz Apellániz et al. 2021; MA22). Here the formalism by El-Badry et al. (2021) was used. There correction was derived for $G < 7$ mag, but it will be used for brighter magnitudes as well. The effect is small in any case, $k = 1.10$–1.15 for $G < 10$ mag. Finally, a more stringent cut on the GOF was imposed. The distribution of the GOF of QSOs was discussed in G21, and in that paper an interval from −4 to +5 was chosen for acceptable solutions. Here the upper limit is slightly relaxed to +8, resulting in a sample of 20 objects. This is consistent with the other often-used selection criterion of RUWE <1.4, which would result in 23 objects.

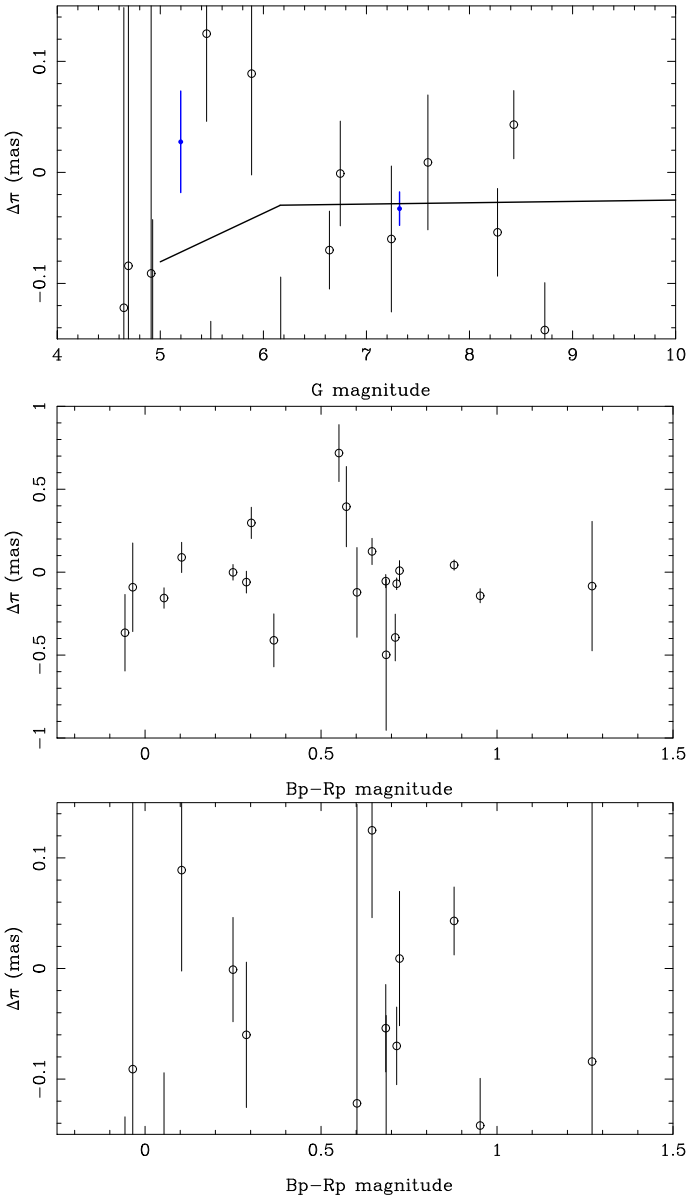

Fig. 3. Parallax difference. Top panel: as Fig. 2 for the final selection as described in the text. There are points outside the plot range. Middle panel: offset plotted against Bp-Rp colour. The ordinate is chosen to be ±1 mas to show all data points in the sample, and the bottom panel has the same range in ordinate as in the top panel.

Model 9 in Table 3 gives the results, and they are displayed in Fig. 3. This figure also shows the offset as a function of Bp-Rp colour with the range in ordinate chosen to show all objects, indicating that there is no evident dependence on colour. Models 10–16 show the results after applying the various correction methods. The results are very similar as before. All three proposed models bring the differences closer to zero, and consistent with zero within the error bars. When restricted to G magnitudes fainter than 6, G21 again provides the correction closest to zero for HEALPix level 2. Nevertheless, most of the results suggest that the corrections may be slightly underestimated (i.e. should be more negative), at least on average over the 6–10 magnitude range.

Table 3. Parallax differences for different assumptions.

Model	$\Delta\pi$ (μas)	G (mag)	N	Model	$\Delta\pi$ (μas)	G (mag)	N	Remarks
	Standard selection (SS)				Final selection (FS)			
1	−41.7 ± 10.7	6.5	68	9	−26.7 ± 14.3	6.2	20	All
	−119 ± 55.4	4.1	27		+78.9 ± 41.1	5.3	12	$G < 5$ (SS), 4–6.2 (FS)
	−93.4 ± 33.7	5.6	11		−41.1 ± 15.3	7.5	8	G = 5–6 (SS), 6.2–10.6 (FS)
	−16.2 ± 16.0	6.6	14					G = 6–7.4
	−71.4 ± 18.3	8.4	8					G = 7.4–9.2
	+52.2 ± 39.4	13.9	8					$G > 9.2$
2	−8.7 ± 11.5	9.0	30	10	−7.7 ± 15.1	7.3	9	All, L21 correction
	+7.8 ± 16.0	6.6	14					G = 6–7.4
	−48.3 ± 18.3	8.4	8					G = 7.4–9.2
	+75.6 ± 39.4	13.9	8					$G > 9.2$
3	−7.6 ± 11.5	9.0	30	11	−8.8 ± 15.1	7.3	9	All, MA22 correction
	+15.5 ± 16.0	6.6	14					G = 6–7.4
	−57.0 ± 18.3	8.4	8					G = 7.4–9.2
	+82.6 ± 39.4	13.9	8					$G > 9.2$
4	−5.6 ± 10.9	8.1	41	12	+10.0 ± 14.5	6.6	15	All, G21, HEALPIx level 0 correction
	−37.5 ± 34.2	5.6	11					G = 5–6 (SS)
	+14.1 ± 16.1	6.6	14					G = 6–7.4
	−40.4 ± 18.3	8.4	8					G = 7.4–9.2
	+79.1 ± 39.4	13.9	8					$G > 9.2$
5	−7.1 ± 10.9	8.1	41	13	+9.5 ± 14.5	6.6	15	All, G21 level 1 correction
	−41.0 ± 34.2	5.6	11					G = 5–6 (SS)
	+13.4 ± 16.1	6.6	14					G = 6–7.4
	−42.2 ± 18.4	8.4	8					G = 7.4–9.2
	+76.5 ± 39.4	13.9	8					$G > 9.2$
6	−8.3 ± 11.2	8.2	39	14	+10.8 ± 15.0	6.7	14	All, G21 level 2 correction
	−58.3 ± 37.8	5.6	10					G = 5–6 (SS)
	+11.7 ± 16.5	6.7	13					G = 6–7.4
	−40.4 ± 18.5	8.4	8					G = 7.4–9.2
	+78.6 ± 39.6	13.9	8					$G > 9.2$
6a	−3.5 ± 11.7	9.1	29	14a	+0.5 ± 15.4	7.3	9	G21, level 2 correction, $G > 6$ mag
7	+5.6 ± 12.4	8.4	35	15	+11.4 ± 17.1	6.7	10	All, G21, level 3 correction
	−45.8 ± 46.0	5.6	9					G = 5–6
	+52.3 ± 19.7	6.6	10					G = 6–7.4
	−44.9 ± 18.8	8.4	8					G = 7.4–9.2
	+80.2 ± 39.8	13.9	8					$G > 9.2$
8	+18.2 ± 13.6	8.6	33	16	+24.9 ± 19.8	6.9	8	All, G21, level 4 correction
	−65.2 ± 47.3	5.6	8					G = 5–6
	+99.6 ± 24.2	6.6	9					G = 6–7.4
	−38.3 ± 19.5	8.4	8					G = 7.4–9.2
	+97.2 ± 40.8	13.9	8					$G > 9.2$

Notes. Results are given for the SS (Cols. 1–4) and the FS (Cols. 5–8), and give the model number, the weighted mean parallax difference with error, the average G-mag of the objects in the bin, and the number of objects considered. Remarks and further details are given in Col. 9.

4. Conclusions

The results from the NSS analysis specific to GDR3 show the potential but also the limitations of the current release. Of the sample of 186 known binaries compiled from the literature to have an orbital parallax, only 8 have an astrometric and 13 have an spectroscopic orbit determined from the NSS analysis. Most objects are eliminated at the pre-filtering stage of the NSS analysis. The analysis of the parallax difference between *Gaia* and orbital parallax is therefore strongly influenced by the large GOF parameter in the main astrometric catalogue, limiting the number of useful objects. The PZPO corrections proposed by L21, G21, and M22 give similar residuals. After these corrections were applied the remaining parallax differences were formally consistent with zero within the error bar for all three recipes. The current data and analysis therefore do not prefer a particular PZPO correction scheme over the other two.

Several improvements may be anticipated in the near future. The number of systems for which an orbital parallax will become available will likely grow, or orbital elements of existing systems will improve. For about one-third of the systems, separate astrometric and spectroscopic orbits exist that were used to obtain the orbital parallax. For consistency, the existing data could be combined to obtain a single solution.

The situation might improve by DR4. The orbital parallax for 18 out of 20 stars in the final selection sample is accurate to better then 5%, and is even better than the *Gaia* value for 6 stars. In the full sample, 148 stars have an orbital parallax

determination better than 5%. Having NSS solutions available for a eight times larger sample would lead to a significantly more precise determination of the PZPO at bright magnitudes. Whether this is realistic would depend on how much the criteria in the pre-filtering and post-processing stages could be relaxed. The impact of the former has been discussed, but some of the stars in the sample may also have been eliminated at the latter stage. Halbwachs et al. (2023) mentioned three criteria that have been applied as well. The one on parallax accuracy[4] would eliminate about 45% of the sample. The selection on eccentricity accuracy[5] would eliminate 1% of the sample, and the one on the significance of the photocenter major axis[6] about 4%. Alternatively, with the planned release of the complete astrometric and spectroscopic time-series data with DR4, the community could combine *Gaia* data with literature data in order to obtain the best-determined orbit.

Acknowledgements. MG is grateful to the International Space Science Institute (ISSI) for support provided to the SH0T ISSI International Team (https://www.issibern.ch/teams/shot/). This work has made use of data from the European Space Agency (ESA) mission *Gaia* (http://www.cosmos.esa.int/gaia), processed by the *Gaia* Data Processing and Analysis Consortium (DPAC, http://www.cosmos.esa.int/web/gaia/dpac/consortium). Funding for the DPAC has been provided by national institutions, in particular the institutions participating in the *Gaia* Multilateral Agreement. This research has made use of the SIMBAD database and the VizieR catalogue access tool operated at CDS, Strasbourg, France.

References

Agati, J. L., Bonneau, D., Jorissen, A., et al. 2015, A&A, 574, A6
Anguita-Aguero, J., Mendez, R. A., Clavería, R. M., & Costa, E. 2022, AJ, 163, 118
Babusiaux, C., Fabricius, C., Khanna, S., et al. 2023, A&A, in press, 10.1051/0004-6361/202243790
Bagnuolo, W. G. Jr., Taylor, S. F., McAlister, H. A., et al. 2006, AJ, 131, 2695
Baron, F., Monnier, J. D., Pedretti, E., et al. 2012, ApJ, 752, 20
Boden, A. F., Lane, B. F., Creech-Eakman, M. J., et al. 1999, ApJ, 527, 360
Boden, A. F., Torres, G., & Latham, D. W. 2006, ApJ, 644, 1193
Chan, V. C., & Bovy, J. 2020, MNRAS, 493, 4367
Docobo, J. A., Belega, Y., & Campo, P. P. 2018a, IAUDS Inf. Circ., 196, 1
Docobo, J. A., Campo, P. P., & Abushattal, A. A. 2018b, IAUDS Inf. Circ., 169, 1
El-Badry, K., Rix, H.-W., & Heintz, T. M. 2021, MNRAS, 506, 2269
Fabricius, C., Luri, X., Arenou, F., et al. 2021, A&A, 649, A5
Farrington, C. D., ten Brummelaar, T. A., Mason, B. D., et al. 2014, AJ, 148, 48
Gaia Collaboration (Prusti, T., et al.) 2016, A&A, 595, A1
Gaia Collaboration (Brown, A. G. A., et al.) 2018, A&A, 616, A1
Gaia Collaboration (Brown, A. G. A., et al.) 2021, A&A, 649, A1
Gaia Collaboration (Arenou, F., et al.) 2023a, A&A, in press, 10.1051/0004-6361/202243782
Gaia Collaboration (Vallenari, A., et al.) 2023b, A&A, in press, 10.1051/0004-6361/202243940
Gallenne, A., Pietrzyński, G., Graczyk, D., et al. 2018, A&A, 616, A68
Gallenne, A., Pietrzyński, G., Graczyk, D., et al. 2019, A&A, 632, A31
Górski, K. M., Hivon, E., Banday, A. J., et al. 2005, ApJ, 622, 759
Graczyk, D., Pietrzyński, G., Gieren, W., et al. 2019, ApJ, 872, 85
Griffin, R. F. 2012a, J. Astrophys. Astron., 33, 29
Griffin, R. F. 2012b, The Observatory, 132, 309
Griffin, R. F. 2018, The Observatory, 138, 192
Groenewegen, M. A. T. 2018, A&A, 619, A8
Groenewegen, M. A. T. 2021, A&A, 654, A20
Halbwachs, J. L., Boffin, H. M. J., Le Bouquin, J. B., et al. 2016, MNRAS, 455, 3303
Halbwachs, J.-L., Kiefer, F., Lebreton, Y., et al. 2020, MNRAS, 496, 1355
Halbwachs, J.-L., Pourbaix, D., Arenou, F., et al. 2023, A&A, in press, 10.1051/0004-6361/202243969
Hartkopf, W. I., Mason, B. D., & Worley, C. E. 2001, AJ, 122, 3472
Hill, G., Barnes, J. V., Hutchings, J. B., & Pearce, J. A. 1971, ApJ, 168, 443
Huang, Y., Yuan, H., Beers, T. C., & Zhang, H. 2021, ApJ, 910, L5
Hummel, C. A., Armstrong, J. T., Buscher, D. F., et al. 1995, AJ, 110, 376
Jao, W.-C., Nelan, E. P., Henry, T. J., Franz, O. G., & Wasserman, L. H. 2016, AJ, 152, 153
Khan, S., Miglio, A., Mosser, B., et al. 2019, in The Gaia Universe, 13
Kiefer, F., Halbwachs, J. L., Lebreton, Y., et al. 2018, MNRAS, 474, 731
Konacki, M., & Lane, B. F. 2004, ApJ, 610, 443
Layden, A. C., Tiede, G. P., Chaboyer, B., Bunner, C., & Smitka, M. T. 2019, AJ, 158, 105
Lester, K. V., Fekel, F. C., Muterspaugh, M., et al. 2020, AJ, 160, 58
Lindegren, L., Hernández, J., Bombrun, A., et al. 2018, A&A, 616, A2
Lindegren, L., Bastian, U., Biermann, M., et al. 2021, A&A, 649, A4
Maíz Apellániz, J. 2022, A&A, 657, A130
Maíz Apellániz, J., Pantaleoni González, M., & Barbá, R. H. 2021, A&A, 649, A13
Mourard, D., Monnier, J. D., Meilland, A., et al. 2015, A&A, 577, A51
Muraveva, T., Delgado, H. E., Clementini, G., Sarro, L. M., & Garofalo, A. 2018, MNRAS, 481, 1195
Nemravová, J. A., Harmanec, P., Brož, M., et al. 2016, A&A, 594, A55
Pearce, J. A. 1936, PASP, 48, 214
Piccotti, L., Docobo, J. Á., Carini, R., et al. 2020, MNRAS, 492, 2709
Pourbaix, D. 1999, A&A, 348, 127
Pourbaix, D. 2000, A&AS, 145, 215
Pourbaix, D., Tokovinin, A. A., Batten, A. H., et al. 2004, A&A, 424, 727
Ren, F., Chen, X., Zhang, H., et al. 2021, ApJ, 911, L20
Riello, M., De Angeli, F., Evans, D. W., et al. 2021, A&A, 649, A3
Riess, A. G., Casertano, S., Yuan, W., et al. 2018, ApJ, 861, 126
Riess, A. G., Casertano, S., Yuan, W., et al. 2021, ApJ, 908, L6
Stassun, K. G., & Torres, G. 2018, ApJ, 862, 61
Stassun, K. G., & Torres, G. 2021, ApJ, 907, L33
Tokovinin, A. A. 1993, Astron. Lett., 19, 73
Tokovinin, A. A. 2016a, AJ, 152, 10
Tokovinin, A. A. 2016b, AJ, 152, 11
Tokovinin, A. A. 2021, IAUDS Inf. Circ., 203, 1
Tokovinin, A. A. 2022, AJ, 163, 161
Tokovinin, A. A., Gorynya, N. A., & Morrell, N. I. 2014, MNRAS, 443, 3082
Tokovinin, A. A., Everett, M. E., Horch, E. P., Torres, G., & Latham, D. W. 2019, AJ, 158, 167
Torres, R. M., Loinard, L., Mioduszewski, A. J., et al. 2012, ApJ, 747, 18
van Leeuwen, F. 2008, VizieR Online Data Catalog: I/311
Wang, X., Ren, S., & Fu, Y. 2015, AJ, 150, 110
Xu, S., Zhang, B., Reid, M. J., Zheng, X., & Wang, G. 2019, ApJ, 875, 114
Zinn, J. C. 2021, AJ, 161, 214
Zinn, J. C., Pinsonneault, M. H., Huber, D., & Stello, D. 2019, ApJ, 878, 136

[4] $\pi/\sigma_\pi > 20\,000/P$ (days), using the orbital parallax to evaluate the inequality.
[5] $\sigma_e < 0.182 \log P - 0.244$.
[6] $a_0/\sigma_{a_0} > 158/P$ (days), but using the major axis of the true orbit instead to evaluate the inequality.

Appendix A: Additional tables

Table A.1. Parameters for the WBS sample

Name	$\pi_{\rm orb}$ (mas)	Sep ($''$)	Source ID	π (mas)	GOF	RUWE	G (mag)	NSS	Flag
01028+3148	8.859 ± 0.203	56.4	314142124302719744	8.495 ± 0.051	1.876	1.083	16.027	0	y
02057−2423	22.331 ± 1.457	56.6	5121561759597725440	21.028 ± 0.019	-2.238	0.910	8.749	0	
02124+3018	11.825 ± 5.068	4.0	300312157810876160	12.738 ± 0.550	139.299	17.831	6.622	0	
02128−0224	24.783 ± 2.616	16.8	2494066897240089984	26.168 ± 0.027	-0.162	0.989	7.582	0	y
02442−2530	22.253 ± 0.158	12.5	5076722404106857472	22.440 ± 0.079	65.411	4.285	8.944	0	y
03396+1823	26.378 ± 2.052	10.1	56861660442751872	27.289 ± 0.045	5.265	1.280	15.005	0	
03400+6352	23.682 ± 1.927	46.2	488099359330834432	23.359 ± 0.018	-1.755	0.951	6.768	0	
04179−3348	18.036 ± 0.112	5.5	4870527586936020864	19.005 ± 0.257	42.199	4.799	13.968	0	y
04247+0442	16.700 ± 0.033	7.1	3283823383389256064	16.800 ± 0.055	30.926	2.686	12.953	0	
04560+3021	6.906 ± 0.353	9.2	156899557664509440	6.718 ± 0.162	0.835	1.026	18.085	0	
08317+1924	77.062 ± 8.257	9.9	662732115407952768	60.248 ± 0.076	27.886	2.051	12.278	0	
09194−7739	14.907 ± 0.299	9.1	5203285503955597184	14.702 ± 0.010	-1.873	0.926	9.277	0	y
09498+2111	3.400 ± 0.879	12.7	640100317815763712	4.729 ± 0.023	0.499	1.017	14.306	0	
12351+1822	9.043 ± 0.362	20.1	3947649169267207296	8.919 ± 0.127	-2.466	0.855	4.690	0	
13196+3507	72.115 ± 29.549	17.8	1473166433840437888	73.923 ± 0.033	17.809	1.678	11.011	0	y
13239+5456	40.497 ± 0.143	14.4	1563590510627624064	40.280 ± 0.285	52.627	3.826	3.914	0	
14206−3753	13.050 ± 0.063	57.4	6116979078226372992	13.233 ± 0.018	3.244	1.179	12.453	0	
14575−2125	170.963 ± 1.697	26.0	6232511606838403968	169.884 ± 0.065	4.937	1.298	5.364	0	
15006+0836	26.385 ± 0.107	34.0	1161798072431380096	25.901 ± 0.114	2.474	1.129	16.967	0	y
15282−0921	50.720 ± 1.212	52.2	6317854118838346752	48.345 ± 0.029	2.005	1.107	7.321	0	
16147+3352	43.980 ± 0.528	7.3	1328866562170960384	44.134 ± 0.018	2.208	1.078	6.438	0	y
16212−2536	6.239 ± 0.131	20.2	6048602103662751488	7.233 ± 0.177	114.633	7.170	8.401	0	
16311−2405	10.466 ± 1.031	13.1	6050627782031927296	7.645 ± 0.020	6.648	1.301	13.015	0	
17038−3809	15.436 ± 0.168	10.6	5976304983594844928	16.084 ± 0.021	6.147	1.230	13.432	0	y
17584+0428	21.666 ± 1.878	18.2	4472789731012862080	23.647 ± 0.022	4.509	1.235	13.349	0	
18002+8000	22.998 ± 0.463	18.7	2294405721759384064	22.434 ± 0.035	3.978	1.230	5.928	0	
18055+0230	194.423 ± 2.677	6.4	4468557611977674496	195.856 ± 0.254	35.917	3.706	5.539	0	y
18058+2127	24.576 ± 0.674	28.2	4576326312901650560	24.694 ± 0.022	29.445	1.787	9.898	0	
18099+0307	20.785 ± 0.552	7.2	4469921487444001792	21.637 ± 0.030	7.282	1.310	11.690	0	y
18339+5144	60.424 ± 0.150	17.0	2145277550935526784	60.590 ± 0.021	5.907	1.238	13.907	0	
18413+3018	8.379 ± 0.250	14.1	4587744672430944512	8.103 ± 0.013	-4.908	0.833	8.699	0	
18501+3322	3.197 ± 0.931	45.8	2090687726329643392	3.513 ± 0.090	44.763	2.862	7.205	0	
19091+3436	28.251 ± 0.853	16.0	2044341077844180736	24.413 ± 0.015	-3.163	0.891	7.879	0	
19196+3720	41.081 ± 0.070	34.6	2051069745406938240	39.318 ± 0.450	337.307	26.510	11.480	0	y
19394+3009	14.766 ± 0.412	4.8	2032457178231864704	12.511 ± 0.132	5.112	1.340	14.046	0	y
21232−8703	14.556 ± 4.288	17.8	6342009495947730432	14.010 ± 0.013	-1.170	0.953	8.826	0	
22038+6438	38.094 ± 2.432	8.1	2218144866573662848	32.184 ± 0.018	-1.464	0.926	6.330	0	y

Notes. Column 1-2: Name and orbital parallax of the main source. Column 3-4: Source Id of the WBS candidate and the separation between the two sources. Column 4-9: parallax (with error), GOF, RUWE, G-mag, and NSS-flag. Column 10: Flag indicating if the star is in El-Badry et al. (2021).

Table A.2. Parameters from the NSS analysis

Name	Source ID	NSS model	π (mas)	σ_π (mas)	Period (d)	σ_P (d)	e	σ_e	GOF	Eff	Sign	K_1 (km s^{-1})	σ_{K_1} (km s^{-1})	K_2 (km s^{-1})	σ_{K_2} (km s^{-1})	a_0 (mas)	σ_{a_0} (mas)
00490+1656	2781872793183604096	SB2			13.82738	0.00027	0.2464	0.0014	8.66	0.45	519.1	60.315	0.116	57.883	0.112		
01096−4616	4933562966514402176	SB2			24.60049	0.00075	0.1896	0.0020	20.15	0.48	286.3	48.734	0.170	51.756	0.172		
03147−3533	5047189109469319680	SB2			75.63557	0.00343	0.0382	0.0020	47.40	0.32	406.3	39.852	0.098	39.858	0.082		
03396+1823	56861694804053120	SB2			6.81420	0.00007	0.4198	0.0035	36.56	0.40	176.8	69.329	0.392	74.454	0.379		
03566+5042	250437313946591360	SB2			30.43678	0.00089	0.6488	0.0018	37.53	0.43	267.4	52.180	0.195	51.924	0.190		
04179−3348	4870527586937201408	SB2			0.97019	0.00001	0.4518	0.0094	35.52	0.66	73.2	50.605	0.691	43.662	0.843		
04247+0442	3283823387685219328	OTS	16.518	0.024	156.34427	0.15026	0.8978	0.0663	0.71	0.00	11.0					3.430	0.313
04469−6036	4677731006145097984	SB2			14.90132	0.00026	0.1965	0.0026	12.04	0.47	281.3	56.339	0.200	56.132	0.201		
04506+1505	3404812685132622592	FDTSB1							1.53								
12313+5507	1571145907856592768	OTS	39.605	0.019	1093.35755	5.22279	0.5371	0.0027	0.28	0.00	110.2					26.812	0.243
14104+2506	1257529526205454336	SB2			9.60584	0.00005	0.1996	0.0010	43.06	0.59	617.5	67.241	0.109	69.392	0.105		
16057−2027	6244076338858859776	OTS	54.476	0.025	105.82585	0.05186	0.1731	0.0166	1.00	0.00	173.3					4.734	0.027
17038−3809	5976304987919824384	OTS	16.114	0.030	7.49295	0.00264	0.2412	0.1685	0.50	0.00	8.5					0.310	0.037
17422+3804	1342735149009387136	OTS	25.197	0.022	1236.58598	39.37131	0.0607	0.0222	0.70	0.00	34.7					12.454	0.359
17422+3804	1342735149009387136	SDTSB1							1.49								
18339+5144	2145277550935525760	OTS	60.620	0.023	32.26596	0.03200	0.1077	0.0767	0.86	0.00	17.4					1.454	0.083
18339+5144	2145277550935525760	SB2			5.97735	0.00013	0.3555	0.0061	33.34	0.64	140.5	34.284	0.244	30.652	0.223		
19264+4928	2129771310248902016	ASSB1	40.881	0.018	166.76852	0.08022	0.1342	0.0077	3.07	0.00	217.2					4.271	0.020
19399−3926	6690041553622067328	SB1			11.41470	0.00042	0.0867	0.0080	2.35	0.32	112.4	42.009	0.374				
20329+4154	2067948245320365184	Orb	46.052	0.021	57.34178	0.02049	0.3118	0.0185	5.08	0.26	184.9					4.406	0.024
23456+1309	2770028132375790976	SB2			19.89153	0.00086	0.3655	0.0026	40.21	0.57	164.4	39.733	0.242	29.740	0.241		
23485+2539	2852594583674129152	SB1			977.91854	104.31029	0.5867	0.1500	1.58	0.31	8.9	1.188	0.134				
23571+5542	1994714276926012416	SB2			12.15694	0.00011	0.3156	0.0016	10.97	0.46	347.7	71.700	0.206	72.416	0.207		

Notes. Column 1: Name. Column 2: Source Id. Column 3: NSS model. OTS stands for OrbitalTargetedSearch, ASSB1 stands for AstroSpectroSB1, Orb stands for Orbital, FDTSB1 stands for FirstDegreeTrendSB1, SDTSB1 stands for SecondDegreeTrendSB1. Column 4-18: parallax, period, eccentricity (with errors), GOF, `efficiency`, `significance`, velocity amplitude of the two components (with errors), photocenter semi-major axis with error.